# PHOTODISSOCIATION OF HYDROGEN HALIDES IN A CRYOGENIC RARE GAS ENVIRONMENT: A COMPLEX APPROACH TO SIMULATIONS OF CLUSTER EXPERIMENTS

PETR SLAVÍČEK AND PAVEL JUNGWIRTH
*J. Heyrovský Institute of Physical Chemistry, Academy of Sciences of the Czech Republic and Center for Complex Molecular Systems and Biomolecules, Dolejškova 3, 18223 Prague 8, Czech Republic*

**Abstract.** Simulation of the photodissociation experiment performed in a large neutral cryogenic clusters is described in this chapter. The emphasize is put on the methodological aspects of the simulations, namely on the correct preparation of the initial state. Possible control of photodissociation process is discussed. The good agreement between theory and experiment not only indicates the quantitative predictive power of the calculations, but also confirms that the experimental concepts and analysis of cluster production in supersonic beams are quite reliable.

## 1. Introduction

Photodissociation of small molecules in different cluster environments has attracted much attention in recent years. The reason is the possibility to explore physical properties as a function of a cluster size. One can thus address the question of the onset of surface and bulk solvation. Moreover, for molecular cluster certain quantities such as the kinetic energy distribution of the photodissociated fragments are experimentally available and direct comparison with theoretical calculations is feasible. Hydrogen halide molecules interacting with different rare gas clusters have served as a prototypal systems for such investigations using different levels of theoretical treatment [1, 9, 16, 28, 30, 31, 33, 34, 37, 38, 42, 43, 46, 54, 55]. Photodissociation in a cryogenic rare gas environment have several appealing features from the theoretical point of view. First, rare gas atoms serve as simplest, structureless solvents. Rare gas atoms exhibit only elementary features of solvation. Basically, the only important solute-solvent interaction is the repulsion between the photodissociation fragments and the rare gas atoms. Second, under cryogenic conditions the system is usually prepared in a well defined state. We can thus avoid complications connected with averaging over thermodynamical distributions. On the other hand, nuclear quantum effects such as the zero point energy motion can play a crucial role.

Recently, a lot of new experimental results in supersonic beams have been produced in this field [9]. The basic setup of a cluster experiment is following. First, the clusters are prepared in a supersonic beam. Second, the clusters are photodissociated by a polarized laser beam, and, third the photodissociated fragments are ionized and detected by techniques of mass spectrometry.

The experimental setup has its counterpart in the theoretical methodology. First, the doped cluster has to be prepared. In theory this means to construct the multidimensional potential energy surface for the interaction of particles in the ground state (even simple systems like Lennard-Jones clusters can form surprisingly rich energy landscapes). The potential energy surface of the HX-$Rg_n$ system can be constructed from the known interactions between cluster fragments. If these are not available, it is required to calculate them by means of *ab initio* quantum chemistry methods. The cluster is prepared under cryogenic conditions and quantum vibrational and rotational effects can thus be of a vital importance. The initial ground state wavefunction of the system is constructed. Since we deal with large systems, usually approximations are applied. The experiment is, however, not performed at T = 0 K, therefore, we have to ask what is the role of entropic effects on the initial state of the doped cluster. The thermodynamical averaging via a certain simulation tool, e.g., molecular dynamics, is thus performed.

The second experimental step is photodissociation. From a theoretical point of view this means (i) changing the potential energy surface of the system and (ii) time evolution of the system. As for the ground state, also after the photoexcitation the potential energy surface has to be constructed from known or calculated interactions between cluster fragments. In the excited state, open shell systems occur. A simple and elegant method for the construction of the potential energy surface of large systems containing an open shell particle is the Diatomics-in-Molecules approach. Then, an appropriate method has to be chosen for the dynamics. Fully quantum description of the dynamics is not computationally feasible and certain approximations have to be adopted. Approximations can basically go in two directions. The first one is to connect the quantum dynamics with its classical counterpart. The second option is the factorization of the problem. The actual choice depends not only on the system under study but also on the type of questions we raise. A certain level of treatment is used when the dominant quantum effect is the change in the energetics, while a different approach is used if interference and coherence effects are of interest.

The third step in the experiment is detection. On the simulation side this is equal to visualizing the results. A time evolution of the calculated wavefunction (or a swarm of classical trajectories) has to be translated into a physically meaningful pictorial representation. Finally, at this stage we should link our simulations with the measurements. This means to find measurable quantities which can be compared with the experiment. We can calculate quantities both in the time and in the energy domain. Both can be in principial reached experimentally.

In this chapter we concentrate namely on the methodological aspects of the simulations of photodissociation process in large clusters. The aim is, however, not only to describe the process but also to address the question about how to actively influence the process, i.e., how to control photodissociation by employing weak forces, external fields or an IR laser pulse.

The organization of this chapter follows the above mentioned division: in section 2 we discus the theoretical tools for initial state description, section 3 describes the methodology of photodissociation simulations in extended systems, in section 4 we describe the analysis of experimental results and in section 5 we discuss the possible control of photodissociation process.

## 2. Preparation of clusters

As is further stressed in section 5, the initial state of the cluster, i.e., the state prior to the photodissociation is of a fundamental importance for the subsequent photodissociation dynamics. The determination of the initial cluster structure consists of three steps: first we find the optimized structure, i.e., the minimum on the potential energy surface of the ground state. In a second step, we calculate the ground state vibrational wavefunction. This second step can qualitatively change the initial structure. The final step is to explore what is the distribution of isomers at a thermodynamic equilibrium corresponding to experimental temperature. Even though this temperature is quite low, its non-zero value may play a significant role for weakly bound clusters.

### 2.1. OPTIMAL STRUCTURES

For finding optimal classical structures it is first required to construct reliable potential energy surface for the system in the ground state. Usually, several approximations are employed. First, we neglect three body interactions within rare gas atoms, and second we assume that the interaction between the hydrogen halide and the rare gas atom is within a certain range independent of the HX bond distance. The latter approximation is not necessarily always justified [10]. With these approximations we can write the PES of a HX-Rg$_n$ cluster as a following sum

$$V(HX - Rg_n) = \sum_{i=1,n} V_{HX-Rg} + \sum_{i=1,n} \sum_{j=i,n} V_{Rg-Rg} + V(HX), \qquad (1)$$

where $V_{HX-Rg}$ is a three body term for the interaction between a rare gas atom and a hydrogen halide molecule with a fixed bond length, $V_{Rg-Rg}$ is a pair rare gas-rare gas potential and $V(HX)$ is a potential of HX in the $^1\Sigma$ state. The last term is taken either within the harmonic approximation or as a Morse function [19]. The expression 1 has been found to provide good estimates of structural properties of larger HX-Rg$_n$ clusters [3]. The terms $V_{HX-Rg}$ and $V_{Rg-Rg}$ are often known with experimental or semi-experimental accuracy. If experimental information is missing, we calculate these terms by mean of *ab initio* methods.

To find the classical structure of a molecular cluster basically means a minimization of the potential energy function 1. Since we treat systems with as many as 300 particles, this task is generally very difficult to perform. Even for a simple potential form the energy landscape becomes soon very complicated with many local minima which are rather close in energy [51]. We have performed the optimization in two steps: in the first one we have obtained the optimized structure of the impurity free rare gas cluster. Then we have chosen a position where the dopant is placed and we have locally re-optimized the structure.

Once we have a structure of the rare gas cluster, we have to decide into which position the dopant is placed. On Fig. 1 all the possibilities are described. The dopant may occupy a smooth adsorption site, i.e., it can stay on the surface of the cluster, interacting thus basically only with three nearest neighbors (1). Other position is the substitutional surface place, in which the dopant replaces one of the rare gas atoms from the most outer shell (2). The cluster can replace the central argon atom of the cluster (3), or can be placed also in the subsurface substitutional place (4). After adding the dopant, a local optimization is performed. The choice of the dopant position should reflect the way the cluster is prepared, either by a pick-up procedure or by co-expansion. Under experimental conditions we may expect both the surface and the embedded isomers to be kinetically stable even though the global minimum can be energetically well bellow the second isomer. This turns out to be the case of argon clusters. For the weakly bound neon clusters, however, one has to be cautious. At the experimental temperature the dopant can be distributed over several positions.

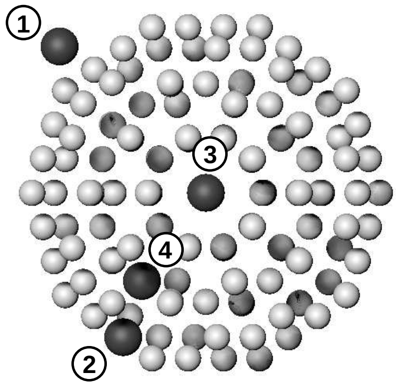


*Figure 1.* Possible positions of the HX dopant in or on the surface of large rare gas cluster. 1. Smooth adsorption, 2. Incorporation in the surface, 3. subsurface solvation, 4. Central solvation.

## 2.2. INITIAL VIBRATIONAL WAVEFUNCTION OF LARGE CLUSTERS: SEPARABLE APPROACH AND DIFFUSION MONTE CARLO METHOD

The quantum delocalization of the particles has two consequences for the photodissociation experiment. First, the smearing of the initial state changes the sampling statistics during the photodissociation. This is especially important for the HX librational motion. This motion has a highly delocalized character (e.g., the dopant inside the cluster cage the HX behaves almost as a free rotor). Starting the dynamical calculations from the minimum of the potential energy surface has then little physical justification. We discuss in more detail this issue in the next chapter. Another consequence of the quantum delocalization is that one is forced to rethink the concept of structure in certain molecular clusters.

For a correct description of the cluster state at a temperature T=0 K it is, therefore, inevitable to treat the effect of quantum delocalization. Technically, this means to solve the N-dimensional vibrational Schrödinger equation. One can calculate the ground state wavefunctions for systems of interest either exactly (for small systems) or by dividing the system degrees of freedom into several groups and treating them separately. Finally, one can calculate the exact N-dimensional ground state wavefunction by mean of the stochastic Diffusion Monte Carlo method. This method can not, however, be directly used as a starting point for the subsequent quasi-classical molecular dynamics simulations, and it is also not straightforward to extend this method for excited states calculations. In following paragraphs, we briefly describe the employed methodology of the vibrational calculations. Generally, we aim to solve the stationary Schrödinger equation

$$\hat{H}_I \Psi_0 = E_0 \Psi_0, \tag{2}$$

where

$$\hat{H}_I = \sum_{i=1,n} \hat{T}_{Ar,i} + \hat{T}_X + \hat{T}_H + V_{GS}(HX - Rg_n). \tag{3}$$

Here $\hat{T}$ stands for the kinetic energy operator and $V_{GS}(HX - Rg_n)$ is the potential energy surface in the ground state. The first approximation which we introduce is a separation of the fast HX vibrational (stretching) motion from all other degrees of freedom. The HX distance is thus held constant during the calculations.

So far, we have only separated out the HX vibrational motion. Generally, such a solution of the stationary Schrödinger equation is not computationally feasible for clusters with more than one argon atom. Therefore, other approximations have to be employed. At the same time, all phenomena important for the cluster structure have to be properly included. We have performed an adiabatic separation of the HX librational motion from the motion of the heavy particles, i.e., from the cage modes. Moreover, the cage modes have been calculated within the harmonic approach, i.e., by a diagonalization of the Hessian matrix. Formally, the wavefunction is expressed as

$$\Psi(\rho, q_1, q_2, ...., q_{3n-6}, \Theta, \Phi) = \frac{\chi(\rho)}{\rho} \phi_1(q_1)....\phi_{3n-6}(q_{3n-6}) \phi_{lib}(\Theta, \Phi, \{q_i\}), \tag{4}$$

where $q_i$ are the normal coordinates of cage (i.e., heavy atoms), and $\rho$ is the H-X separation. The factor $1/\rho$ comes from the use of spherical coordinates. As has been already said, the cage modes are taken into account within the harmonic approximation, while the librational wavefunction of the HX molecule $\phi_{lib}(\Theta, \Phi)$ is calculated by a diagonalization of the HX (hindered) rotational Hamiltonian in the basis of spherical harmonics

$$\hat{H}_{rot} = \frac{\hbar^2}{2\mu_2 r^2} \hat{j}^2 + V(\Theta, \Phi, \{q_i\}). \tag{5}$$

The term connected with the overall rotation of the cluster is neglected since $\mu_1 R^2$ is much larger than $\mu_2 r^2$. Due to the loss of cylindrical symmetry the potential V becomes also $\Phi$–dependent. Both the potential for the hindered rotation of HX and the librational wavefunctions are parametrically dependent on the cage coordinates.

This approach is satisfactory for systems, where the minima corresponding to HX–$Rg_n$ and XH–$Rg_n$ structures are well separated or correspond to similar heavy atom geometries and, therefore, we can separate the librational and cage modes. The energy gap between minima corresponding to possible isomeric structures is increasing with the number of rare gas atoms. Thus, the coupling between vibration and internal rotation does not usually have a strong effect on the ground state structure of the explored complexes (Ar$\cdots$HI and Ne$\cdots$HI), however, it can seriously influence the bound states. Another concern is connected with the role of cage anharmonicity.

Principally exact solution of the vibrational Schrödinger equation can be found by applying the Diffusion Monte Carlo method. Diffusion Monte Carlo (DMC) is a method for the numerical treatment of many-body quantum systems which exploits an isomorphism between the time dependent Schrödinger equation

$$\imath\hbar \frac{\partial \Psi(\vec{r},t)}{\partial t} = \left\{ -\frac{\hbar^2}{2} \sum_{j=1}^{n} \frac{1}{m_j} \nabla_j^2 + \{V(\vec{r}) - E_{ref}\} \right\} \Psi(\vec{r},t) \tag{6}$$

and a multidimensional diffusion equation with anisotropic diffusion coefficients

$$\frac{\partial C(\vec{r},t)}{\partial t} = \left\{ \sum_{j=1}^{n} D_j \nabla_j^2 - k(\vec{r}) \right\} C(\vec{r},t) \ . \tag{7}$$

These two equations are identical providing that we substitute the real time t for imaginary time $\tau$=it. Recall that the asymptotic solution of the imaginary time Schrödinger equation is the ground state wavefunction of the Hamiltonian. At the same time, we know that diffusion equation describes Brownian motion of discrete micro-particles in the continuum limit. We can, thus, represent the wavefunction by ensemble of random walkers.

The DMC method is in principle exact, the accuracy for ground state calculations being limited only by the statistical noise, which can be reduced to a desired level by a sufficient investment of computer time. No approximations beyond the concept of the existence of a potential surface are thus introduced in vibrational calculations. The low power polynomial scaling of the computational effort of this method with increasing system size makes it very attractive for an accurate treatment of large clusters.

A particularly interesting property is the possibility to obtain results (energies, wave functions and expectation values) with an accuracy which is independent of the system size. This allows an unbiased study of the evolution of cluster properties with size, which is of a particular importance for the present study.

We demonstrate the importance of proper description of initial vibrational wavefunction on the case of small $HI(Ar)_n$ complexes [42]. For the correct description of $HX$-$Rg_n$ photodissociation dynamics the HX librational wavefunction $\phi_{lib}$ is the key component of the vibrational wavefunction. If the hydrogen halide molecule is embedded in the cluster, we observe an almost free rotation of HI. This is a consequence of the high symmetry of this solvation site and the short range character of the van der Waals forces. On the other hand, the HI molecule on the surface of an argon cluster is strongly oriented. This is caused by the asymmetry of the surface site. To properly describe the orientation of the HI molecule on the surface of an argon cluster is not trivial. The interaction potential between HI and argon manifests two collinear minima. The lower minimum corresponds to the H-I...Ar arrangement while the secondary minimum has a hydrogen atom pointing towards the argon atom (I-H...Ar). The first minimum is energetically preferred by approximately 50 $cm^{-1}$. After accounting for zero point motions, the ground state energies $D_0$ differs, however, by only 8 $cm^{-1}$ [29]. For the HI-Ar system the hydrogen wavefunction is oriented away from the argon atom. If this would be also the case for larger argon clusters, then no caging can be observed for the surface isomer. The result obtained from the reduced dimensionality vibrational calculations with the Hamiltonian 5 is shown on a Fig. 2. We found a flip of the librational wavefunction when going from $HI$-$Ar_2$ to $HI$-$Ar_3$ cluster, then a back-flip for $HI$-$Ar_4$ (with librational wavefunction pointing outside of the cluster once again). Starting from $HI$-$Ar_5$ all larger clusters are characterized by hydrogen pointing towards the argon cluster. It is important to emphasize that quantum delocalization (i.e., the zero point energy) plays a major role in the determination of the cluster structure.

Since quantum effects are so important in this case, we have decided to re-calculate the ground state wavefunctions for these clusters with the use of Diffusion Monte Carlo Method. This method provides principally the fully coupled ground state wavefunction. A composite Fig. 3 depicts the square of the wavefunction as a function of $\cos\Theta$, where $\Theta$ is the angle between the HI molecular axis and the vector connecting the argon cluster center of mass with the HI center of mass. The librational wavefunction corresponds to hydrogen pointing away from the rare gas atoms for HI-Ar and $HI$-$Ar_2$ clusters. Starting from the $HI$-$Ar_3$ cluster, hydrogen is oriented towards the argon cluster. Unlike the reduced dimensionality calculations,

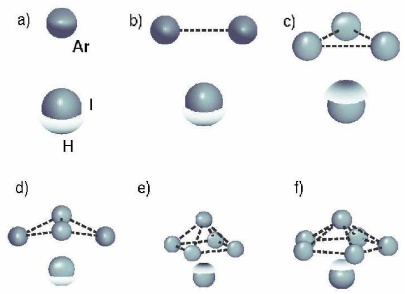


*Figure 2.* Size dependence of the ground vibrational (librational) wavefunction for HI on $Ar_n$ ($n = 1 - 6$). Note the flip of the H wavefunction towards the rare gas clusters upon increasing cluster size. The shadowing represents the angular hydrogen probability and the wired spheres correspond to effective radii of the heavy atoms. For the sake of clarity, the radius of the hydrogen sphere is artificially expanded.

the change is gradual and there is still some wavefunction component with the hydrogen atom pointing outside of the cluster for the HI-$Ar_3$ cluster. No back-flip at HI-$Ar_4$ is observed. We conclude that the general trend of the change of the hydrogen orientation has been confirmed by the DMC calculations, while the back-flip has been found to be an artefact of the previous approximate vibrational calculations. The implications of the size evolution of the librational wavefunction on the photodissociation dynamics are obvious. It suggests that no cage effect should be observed upon photodissociating the HI-Ar complex. Indeed, no low energy signal in the KED spectrum has been observed for this system [4], while for a similar Ar-HBr cluster a weak single atom cage effect has been observed [39]. On the other hand, the cage effect for larger cluster should be pronounced and this is exactly what has been measured and calculated [41].

One of the goals is to use the results of DMC simulations for subsequent quasi-classical studies of photodissociation process. For this purpose, one needs to have a swarm of walkers sampling the square of the wavefunction (or even better a set of walkers in the classical phase space sampling the Wigner distribution). We have reached this goal by the descendant weighting method [25, 6]. DMC sampling of the Wigner distribution is still difficult due to the oscillatory character of the integrand and the problem is still open. Recently, there has been an attempt to overcome the difficulties by approximative separating of the momentum and coordinate space probability distributions, which are evaluated by the DMC wavefunction [5]. This approach, however, is not universal.

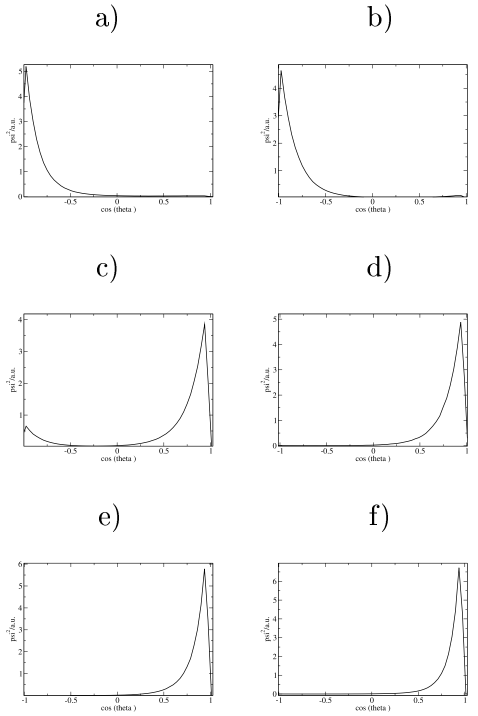


*Figure 3.* Size dependence of the DMC calculated ground vibrational (librational) wavefunction for HI on $\mathrm{Ar}_n$ ($n = 1-6$, corresponding with labels a) to f)). Wavefunction is depicted as a function of $\cos\Theta$ where $\Theta$ is the angle between the cluster center of mass and the center of mass of the dopant. Note the flip of the H wavefunction towards the rare gas clusters upon increasing cluster size seen for the calculations in reduced dimensionality is no more observed.

## 2.3. SIMULATION OF PICK-UP PROCEDURE AND PHASE BEHAVIOR ANALYSIS

Mixed molecular clusters can be prepared by two different techniques: (i) by a co-expansion, where a mixture of the dopant with a rare gas is expanded into the vacuum, or (ii) by a pick-up procedure, in which case the neat rare gas clusters prepared by a supersonic expansion travel through a chamber with a dopant and a buffer gas. For solid systems one is thus able to prepare clusters with the dopants in different positions in or on the cluster according to the way of preparation. However, for ergodic systems (e.g., for liquids) the final dopant sites are simply given by the equilibrium thermodynamical distributions, and they are thus independent of the cluster preparation. The question concerning the degree of ergodicity is interesting particularly in the case of pick-up procedure. The dopant can significantly increase the temperature in this case and even liquidify an originally solid cluster. Molecular dynamics simulation can help in answering the question what is the distribution of positions under experimental conditions corresponding to the pick-up process. A few studies have been performed for argon clusters by means of classical molecular dynamics [35, 48, 49]. Classical molecular dynamics has a limited validity for neon clusters with intermediate quantum effects. Indeed, these quantum effects influence the binding energy per particle (the ground state binding energy is only about 60% of the well depth for a neon dimer) and the mean particle distances and will foreseeably have an important effect on the dopant embedding dynamics, the dopant mobility inside the cluster, and the number of neon atoms evaporating after an impact. For description of these clusters, dynamical methods accounting for at least the principal quantum effects have to be used.

Molecular dynamics is an appropriate tool for the study of the pick-up procedure. It is imperative to perform dynamical (and not thermodynamical) simulation because (i) we do not know in forward the final temperature of the system and (ii) for non-ergodic systems the final distribution can represent just a local minimum on the free energy surface of the system, i.e., a metastable state with a high kinetical stability. Molecular dynamics simulations can thus provide an important insight into the character of clusters under experimental conditions, and at the same time simulations can serve for testing (ground state) potentials.

A powerful method of describing the thermodynamics of quantum systems is based on path integral formulation of the quantum mechanics [15]. The technique, called Path Integral Monte Carlo (PIMC) [8], takes the advantage of the importance sampling via random motion. PIMC has been successfully applied to a study of small neon clusters and their phase behavior [11]. We have, however, already argued that even though the simulation is practically equilibrium, there is a need for a dynamical description in order to properly describe initial conditions during the pick-up procedure and also to account for states which are only kinetically stable.

Full quantum dynamical simulation of dynamic properties of neon clusters at finite temperature is impossible with present computational techniques. This would mean to propagate density matrix which is computationally challenging task. Thus we now face a question how to simulate the quantum systems using essentially classical equations of motion.

In their book on path integrals in quantum mechanics Feynman and Hibbs [15] introduced an effective quantum potential. Its is a temperature dependent potential with which the classical partition function is equal to its quantum counterpart. The so called Gaussian Feynman-Hibbs potential has a form

$$V_{GFH}(|\mathbf{r}|) = \left(\frac{6\mu}{\pi\beta\hbar^2}\right) \int_{\infty}^{-\infty} \int_{\infty}^{-\infty} \int_{\infty}^{-\infty} V_C(|\mathbf{r}+\mathbf{u}|) \exp\left(-\frac{6\mu}{\beta\hbar^2}\right) \mathbf{u}^2 d\mathbf{u} \tag{8}$$

where $V_C$ is a classical potential, $\mu$ is a reduced mass and $\beta = 1/kT$. Feynman-Hibbs could be a good choice for our purpose. However, this method is suited to describe bulk properties. Quantum effects are of higher importance for clusters and Feynman-Hibbs approach may then not adequate. Finally, we need to know the temperature to construct Feynman-Hibbs potential.

We have thus resorted to an approximate technique which attempts to include the above mentioned main quantum effects via the construction of effective potentials $V_q$. Basically, each particle is represented by a single particle wavefunction and the Ehrenfest theorem is applied. Similar ideas have been used with good success even for quantum solids like hydrogen [44]. Effective quantum potentials are also among the results of the Feynman-Hibbs treatment [15] which have been applied to pure neon clusters in the past [40].

While it is possible to construct quantum effective potentials for bulk systems by fitting particle binding energies, bulk densities, and pair correlation functions, our strategy for the construction of the effective quantum potential for clusters avoids the use of empirical information. We use a self consistent iterative procedure, which has been applied previously with surprising success to pure and doped helium clusters [36]. This method is particularly suitable for clusters where empirical density and pair correlation information are unavailable. Conceptually, each particle is replaced by a probability distribution $\phi^2(r)$, centered around its classical position, and assumed to have a spherical symmetry. Starting from the original pair potential $V_{cl}(R) = V_{q,0}(R)$, a delta distribution $\phi_0^2(r)$, and known masses the construction is based on the following sequence of calculations, which is repeated until the $n$-th order potential and distributions have reached self consistency

1. Construction of the pair correlation function $P_n(R)$ between classical particle positions from a classical molecular dynamics simulation at temperature $T$ with the current potential $V_{q;n}(R)$.
2. Convolution of the pair correlation function with the current single particle distribution $\phi_n^2(s)$ according to

$$P_{q;n}(|\mathbf{R}|) = \int P_n(|\mathbf{R}|)\phi_n^2(|\mathbf{R}-\mathbf{R}'|)d\mathbf{R}'. \tag{9}$$

3. Construction of the radial potential $V_{rad;n}(r)$ experienced by each particle in the 'cage' formed by the others by integration over the current

pair potential and the particle distribution following

$$V_{rad;n}(|\mathbf{r}|) = \int V_{cl}(|\mathbf{r} - \mathbf{R}|) P_{q;n}(|\mathbf{R}|) d\mathbf{R}. \tag{10}$$

4. Solution of the radial Schrödinger equation in the radial potential $V_{rad;n}(r)$ in order to find $\phi_{n+1}(r)$ for each particle in the mean field of the others.
5. Construction of the next generation effective pair potential $V_{q;n+1}(R)$ by the convolution

$$V_{q;n+1}(R) = \int \int V_{cl}(|\mathbf{R} + \mathbf{r} - \mathbf{r}'|) \phi^2_{n+1}(|\mathbf{r}|) \phi^2_{n+1}(|\mathbf{r}'|) d\mathbf{r} d\mathbf{r}'. \tag{11}$$

The algorithm was described for a construction of an effective potential for the Ne-Ne interaction. Analogically, one can construct the potential for a Ne-dopant interaction. All radial and pair potentials are computed on a grid and spline interpolated for the molecular dynamics simulations and for the solution of the Schrödinger equation. The number of iterations required to reach self consistency is modest. On Fig. 4 the convergence of the effective potential is shown. The figure depicts the classical potential, the first iteration and the $10^{th}$ iteration which is fully converged. Actually, only 4 iterations are required for a fully converged effective quantum potential in this case. The 'broadening' of each particle described by $\phi_n$ tends to fill in the potential well and leads to a shift to larger mean particle distances clearly accounting qualitatively for the quantum zero point effects. The change in the effective well depth in fact reproduces surprisingly well the amount of zero point energy in the system and the change in mean particle distances accounts very well for the change of the bulk density upon inclusion of quantum effects [36]. The resulting potentials are clearly temperature dependent and could in principle be reconstructed periodically during a non equilibrium impact simulation. This would have sense if we were interested in the first stage of the pick-up process, i.e., in the collision. We address, however, a question what is the final dopant distribution, therefore, this recalculation of the effective quantum potential is not required. Note also that (unlike, e.g., the Feynman-Hibbs potential) our effective quantum potential is size dependent. This corresponds to a fact that smaller systems exhibit generally a stronger quantum character. Thus, this approach is well suited for the study of large moderately quantum clusters.

Figure 5 displays the result of the HBr pick-up on a cluster with 130 neon atoms. The simulation can be visualized in two ways. On Fig. 5a the density of the dopant atom as a function of the distance from the center of mass of the cluster is depicted. For comparison also the density of neon atoms is added in the graph. The majority of the dopant atoms stays in

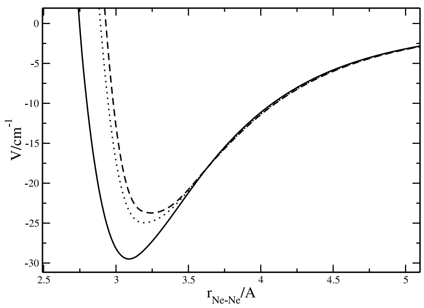


*Figure 4.* Convergence of the Ne-Ne effective quantum potential during its iteration.

the surface area of the cluster, i.e., in the third shell. There is also a peak in the very central position of the cluster. Note, however, that the depicted quantity is a density, which should be multiplied by a factor $4\pi r^2$ to obtain the number of dopant atoms. Thus, only some 7 % of the dopants land in the fully embedded positions. Most of the dopants stay deeply in the third shell, often on the border with a second shell. The $Ne_{130}$ cluster is apparently of a semiliquid character after the impact of the dopant, enabling occasionally the dopant to come to the center. However, the position in the surface is preferred. Another way how to visualize the final solute distribution in the cluster is to display the number of neon atoms in the proximity of the dopant (i.e., closer than 4.3 Å) . The resulting distribution is displayed on Fig. 5b. Fully embedded dopants are those with the number of nearest neighbors larger than 15 (also some of the neon atoms from second solvation layers are occasionally counted). Most of the dopants are interacting with either 6 neon atoms or with around 10 neon atoms (this corresponds to the dopant position between the third and the second layers). There is no evidence for smooth adsorption of the HBr dopant on the neon clusters, in which case, one would expect the HBr molecule to directly interact only with approximately 3 neon atoms.

The situation for $Ne_{300}$ cluster is different. Neon clusters with four solvation layers are much more stiff than clusters with tree layers. Moreover, quantum effects are less important for larger clusters since neon atoms are now more confined. As a result, none of the HBr dopants penetrates into the fully embedded position (corresponding densities for dopant and neon atoms are depicted in Fig. 6a). Most of the HBr particles stay deeply solvated in the outer, fourth neon layer. There is also a small portion (6 %) of dopants in the smooth adsorption position. This amount is, however, too

a) b)

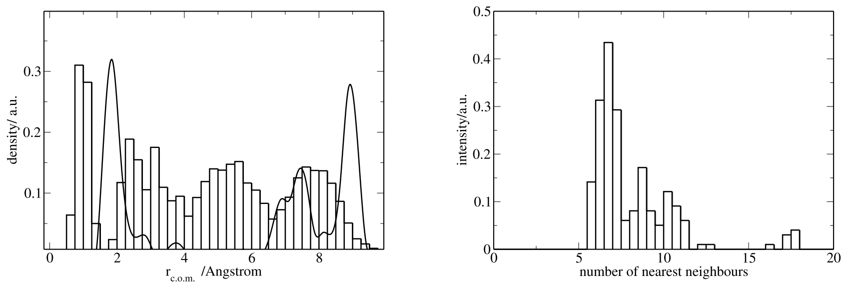


*Figure 5.* Pick-up of HBr on $Ne_{130}$ cluster. a) Density of dopant atoms (solid line) in comparison with the density of neon atoms (histogram). b) Distribution of number of nearest neighbors to the dopant atom.

a) b)

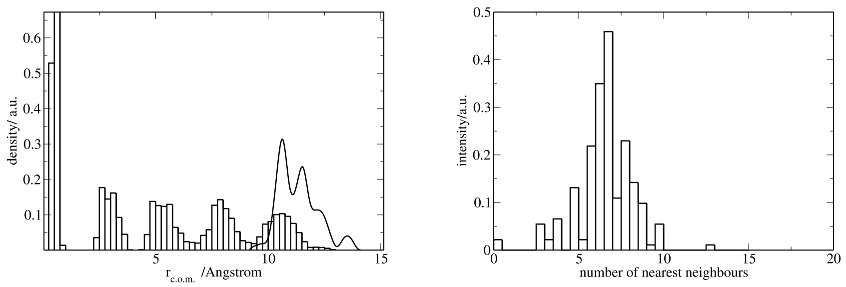


*Figure 6.* Pick-up of HBr on $Ne_{300}$ cluster. a) Density of dopant atoms (solid line) in comparison with the density of neon atoms (histogram). b) Distribution of number of nearest neighbors to the dopant atom.

small to allow to decide whether it is only an artefact of a short duration of the pick-up simulation or whether the occupation of this position actually reflects a genuine thermodynamical distribution. Fig 6b shows the number of nearest neighbors of the HBr dopant for the same system. We can observe the typical feature of the surface solvation with 6-10 solvent atoms closer than 4.3 Å. This result indicates that the cluster is solid after the pick-up of the dopant and the part of the phase space with embedded dopant is virtually not accessible under the experimental conditions.

One of the important issues addressed in our simulations is the character of clusters under study. Are these clusters solid or liquid under experimental conditions? If they are liquid, then the distribution we observe in the pick-up and consequently in the photodissociation simulations corresponds to a statistical distribution at a given temperature. If, however, the cluster is solid then both in the simulations and in the experiment we observe a quasi-stationary state with a very long lifetime rather than an equilibrium thermodynamical state. This question can be resolved by means of the instantaneous normal modes (INM) density of states (DOS) spectrum. To calculate INM DOS we construct the Hessian matrix in a mass-weighted atomic Cartesian coordinate basis of N atoms $x_{n\mu}$ with $\mu=\{x, y, z\}$. For a give instantaneous position $\mathbf{R}$ the Hessian matrix element reads

$$D_{n\mu,n'\mu'}(\mathbf{R}) = \frac{\partial}{\mathbf{x_{n\mu}}} \left( \frac{\partial \mathbf{V}}{\partial \mathbf{x_{n'\mu'}}} \right)_{\mathbf{R}}, \tag{12}$$

where $V$ is the interatomic potential. By diagonalizing of the Hessian matrix we get 3N eigenvalues $\lambda_i$, which are related to harmonic frequencies by a simple relation

$$\omega_i^2(\mathbf{R}) = \lambda_i(\mathbf{R}). \tag{13}$$

At the same time we get also 3N eigenvectors in the form
$c_{1x}, c_{1y}, c_{1z}, c_{2x}, c_{2y}, c_{2z}, .........c_{Nx}, c_{Ny}, c_{Nz}$. These coefficients describe the contribution of each atom to the $i$-th mode. A quantity which is the basic output of the INM procedure is the density of states. This is nothing more than a histogram of frequencies averaged over an ensemble of configurations obtained by molecular simulation techniques:

$$\rho(\omega) = \left\langle \sum_{i=1}^{3N-6} \delta(\omega - \omega_i) \right\rangle . \tag{14}$$

We have omitted the six frequencies corresponding to rotational and translational motions of the whole cluster. One of the advantages of the INM analysis is that we can perform projections of the density of states. One can decompose the density of states spectrum, e.g., into molecular rotational and translational motion [45]. For molecular clusters it is interesting to explore the localization of the motion described by the Hessian eigenvectors at different frequencies. Even though the harmonic motion is inherently collective, certain motions can be attributed to a limited area. This is the case of non-homogeneous systems, where the spectral characteristics can be quite different for different spatial parts. We define a projector $P_{area}$

$$P_{area} = \sum_{n \in area} \sum_{\mu=x,y,z} c_{n\mu}^2, \tag{15}$$

where area can be, e.g., a certain cavity around a host molecule. The projected density of state is then given as:

$$\rho^{area}(\omega) = \left\langle \sum_{i=1}^{3N-6} P_{area}\delta(\omega - \omega_i) \right\rangle . \tag{16}$$

A critical issue is the sampling of instantaneous configurations for the INM analysis. We have sampled the instantaneous configurations via classical molecular dynamics run on effective quantum potentials (the same as we have used for simulating the pick-up procedure).

The typical INM DOS spectrum for a liquid differs significantly from that for a solid. A typical DOS spectrum of an atomic liquid consists of a right triangular pattern for the real frequencies distribution corresponding to translational atomic motion [45]. This shape is caused by a dominant presence of the slow, soft modes in liquids. Furthermore, a significant fraction of imaginary frequencies is present in liquids (imaginary modes are usually depicted for convenience on the negative axis of the DOS spectra). Imaginary frequencies dissappear in solid systems. Moreover, the right-triangular shape of the positive part of the spectrum disappears. The spectrum for an atomic bulk solid shows different spectral features, corresponding to longitudinal and transversal mode peaks. We can see the onset of these features in clusters. They become more important for larger clusters where the fraction of the interior neon atoms is larger. We calculated the INM DOS spectra for clusters of the same size as those in the pick-up simulations, i.e., with 130 neon atoms and with 300 neon atoms. We took the advantage of the projection technique to investigate the phase behavior of the neon atoms in different cluster layers.

Figure 7a depicts the INM DOS of $Ne_{127}$ cluster at 10 K. The DOS of the interior part of the cluster has the imaginary frequencies strongly suppressed. However, there is still a certain fraction of them and we may conclude that a cluster of this size is a border line case, close to the phase transition. This is in agreement with previous experiments on the doped neon clusters [50]. Still, the core of the cluster is more solid than liquid. Moving closer to the surface of the cluster, the character of the density of states changes. Now, it is a typical spectrum for a liquid state with the right triangular shape in the real part of the spectrum and with a significant imaginary frequency contribution.

The INM DOS spectrum for the interior part of the $Ne_{293}$ cluster (Fig. 7b) exhibits feature typical for a solid. Frequency distribution is shifted towards higher values and no imaginary frequencies are observed. This is basically true for all the layers except for the outermost one, which is apparently liquid. We may thus conclude that both clusters explored ($Ne_{127}$ and $Ne_{293}$) have a solid core with a liquid surface. This enables the dopant to be deeply solvated in the surface. The character of the cluster, however,

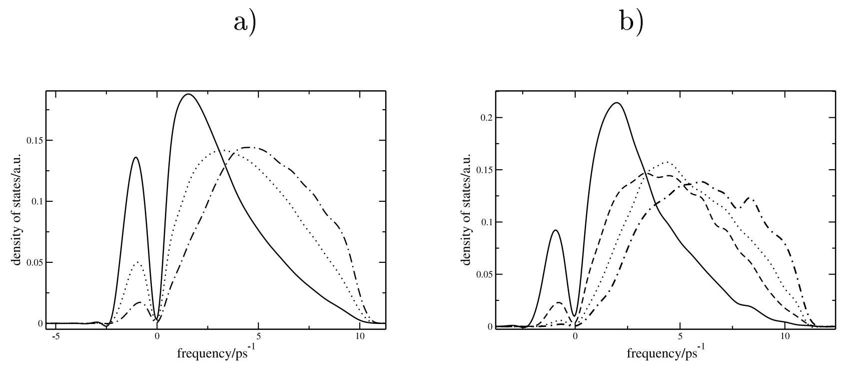


*Figure 7.* INM density of states of different layers in neon clusters. All density distributions are normalized. Imaginary frequencies are displayed on the negative part of the axis. a) $Ne_{130}$ cluster. Outer shell-solid line, medium layer-dotted line, inner part of the cluster-dashed-dotted line. b) $Ne_{300}$ cluster. Outer shell-solid line, third shell-dashed line, second layer-dotted line, inner part of the cluster-dashed-dotted line.

prevents the dopant to penetrate deeper into the inner layers. It is interesting to compare these cluster DOS with those calculated or measured for the bulk (phonon spectrum) [12, 27]. Clusters should represent "the bridge between the isolated molecule and the bulk". Typical bulk features are boson peaks observed in the phonon DOS. We can observe such a feature for the interior neon atoms. However, the convergence to the bulk limit is rather slow. This is not surprising if we assume that even for the largest cluster explored approximately one half of the neon atoms form the outer shell.

## 3. Photodissociation

Once the cluster is prepared in its initial state, described usually by the ground state wavefunction $\Psi_0(\vec{r})$, the exciting laser pulse is switched on. Let's assume for the moment that the laser pulse is infinitely short (we modify this assumption later). This simply means that the whole wavefunction is promoted into the excited state, i.e., the Hamiltonian has instantaneously changed from $\hat{H}_I$ into the excited state Hamiltonian $\hat{H}$. The wavefunction is then no more an eigenfunction of the Hamiltonian $\hat{H}$ and the system starts to evolve according to the time-dependent Schrödinger equation

$$i\hbar \frac{\partial \Psi(\vec{r},t)}{\partial t} = (\hat{T} + \hat{V}(\vec{r}))\Psi(\vec{r},t). \tag{17}$$

If we neglect the spatial dependence of the transition dipole moment, the initial condition for the eq. 17 is

$$\Psi(\vec{r},0) = \Psi_0(\vec{r}). \tag{18}$$

We now face the task to numerically solve equation 17 and to analyze the final wavefunction. Note at this moment that the vector $\vec{r}$ has a dimension $3N$ (N is number of particles). Although there are efficient numerical algorithms for propagating the time-dependent Schrödinger equation both on a grid or in a suitable basis [26], these can hardly be used for systems exceeding several particles. Therefore, we have to choose an approximative way of the solution of the eq.17.

We have to assess how strongly quantum mechanical the system is. A quantity which measure the "degree of the quantum character" of a certain object is the de Broglie wavelength

$$\lambda = \frac{2\pi\hbar}{\sqrt{2mE}} \tag{19}$$

where $m$ is the mass of the object and $E$ is the energy. According to this expression, hydrogen seems to be a good candidate for the strongly quantum part of the system. This is certainly true in the ground state where the energy is small. In the excited state, however, energy of several electronvolts is pumped into the system. Due to this high excess energy the hydrogen atom starts to behave almost classically. For obtaining most of the relevant physical information and insight it is required to describe the initial wavefunction in a fully quantum way, while the subsequent dynamics can be treated classically. Practically, this is performed via the so called *Wigner trajectories* method, which is described in the next section. Finding a connection between quantum and classical mechanics represents one direction of the approximate solution of eq. 17. Wigner trajectories are the crudest example of these techniques. With this method we loose all effects connected with the interferences, e.g., tunneling [1]. To account for these phenomena, we can use approximative quantum methods exploiting the separability of the wavefunction or semiclassical methods from the WKB family.

### 3.1. CONSTRUCTION OF POTENTIAL ENERGY SURFACE

The interaction potential in excited states of the HX-Rg$_n$ clusters has been divided into a non-pairwise X$\cdots$Rg$_n$ component and the remaining pairwise additive interactions

[1] To account for these phenomena while still using the classical law of motion one has to introduce swarm of trajectories which have phase relations among themselves, see reference [13]. Lets also point on the possibility to introduce a phase into a classical autocorrelation function [53]

$$V^\alpha = V^\alpha_{HX} + V(X \cdots Rg) + \sum_{i=1,n} V(Rg \cdots H) + \sum_{i=1,n} \sum_{j=i,n} V_{Rg-Rg}, \quad (20)$$

where the index $\alpha$ denotes the particular HX excited state ($^1\Pi$, $^3\Sigma$ and $^3\Pi$). The interaction potential of the rare gas dimer has been assumed to be the same as in the case of the ground state. The interaction between the rare gas atom and the hydrogen atom has been calculated by *ab initio* methods (see later in this section).

The interaction between an open shell atom with a closed shell atom or molecule can be modeled with the Diatomics-in-Molecule (DIM) method [14]. This is an approximate approach, however, with a sound chemical motivation. The total interaction energy between an open shell atom and all the remaining closed shell atoms in the cluster can be expressed in a pair additive way as

$$V_{DIM} = \sum_{i=1,n} U_i^{DIM}(\vec{r_i}), \quad (21)$$

where $\vec{r_i}$ is the radius vector between the i-th rare gas atom and the p-atom (open shell atom) and $U_i^{DIM}$ is the interaction energy between a single rare gas atom and the open shell atom. The $U_i^{DIM}$ term is expanded in Legendre polynomials, with only two terms contributing

$$U_i^{DIM}(r_i, \gamma_i) = V_0(r_i) + V_2(r_i) P_2(\cos\gamma_i), \quad (22)$$

The potentials are then obtained by a diagonalization of $V_{DIM}$ in a suitable electronic basis ($p_x$, $p_y$, $p_z$ functions).

### 3.2. QUANTUM DYNAMICS OF LARGE CLUSTERS: REDUCED DIMENSIONALITY AND SEMICLASSICAL APPROACH

The time dependent quantum dynamical method based on the assumption of separability is so called TDSCF approach (also called the Time-Dependent Hartree method) [17]. The goal is to find using the time-dependent variational principle the best single particle separable representation of the multidimensional time-dependent wavefunction. Thus, we star with expressing the total wavefunction as

$$\Psi(q_1, ..., q_N, t) = \prod_{j=1}^{N} \phi_j(q_j, t) \quad (23)$$

where the multiplication runs over all modes. Substituting this form of a wavefunction into the ime-dependent Schrödinger equation leads to the following set of one-dimensional Schrödinger equations for the individual degrees of freedom

$$i\hbar\frac{\partial\phi_j(q_j,t)}{\partial t} = [-\frac{\hbar^2}{2m_j}\frac{\partial^2}{\partial q_j^2} + \bar{V}_j(q_j,t)]\phi_j(q_j,t) \tag{24}$$

where the effective single mode potentials $\bar{V}_j$ are defined as

$$\begin{aligned}\bar{V}_j(q_j,t) = &\langle\prod_{l\neq j}\phi_l(q_l,t)|V(q_1,...,q_N)|\prod_{l\neq j}\phi_l(q_l,t)\rangle + \\ &\frac{1-N}{N}\langle\prod_{l=1}^{N}\phi_l(q_l,t)|V(q_1,...,q_N)|\prod_{l=1}^{N}\phi_l(q_l,t)\rangle\end{aligned} \tag{25}$$

.

For the description of photodissociation process we have widely used an extension of TDSCF method called the Classical Separable Potential method, in which the effective potentials are evaluated using classical trajectories [22]. Note that both for the TDSCF and CSP method the configuration interaction extension is possible, although the convergence is very slow. Other approximative methods are based on the use of gaussians or on the path integral formalism of quantum mechanics [23].

### 3.3. CLASSICAL DYNAMICS: WIGNER TRAJECTORIES APPROACH

The method of Wigner trajectories is essentially a purely classical dynamics with a set of initial conditions given by an initial wavefunction. Thus, the only issue in this method is how to properly map the initial wavefunction onto a classical phase space. The coordinate distribution is in quantum mechanics given by a square of the modulus of the wavefunction $|\Psi((\vec{r}))|^2$, analogically we can get the distribution in the momentum space. Due to the Heisenberg uncertainty relations it is impossible to specify *uniquely* coordinates *and* momenta at the same time. This is a principial issue with no analogue in classical mechanics. There are plenty of quantum phase-space distributions and some of them look *almost* like the classical phase-space distribution functions. This problem is more serious for photodissociation than for the collisional processes: the motion in the excited state begins at short distances, in an area where the interaction between modes is the strongest. A small change in the initial conditions may cause a huge change in the final distribution.

The distribution which is most widely used is the so called Wigner distribution function [20]. It is defined as

$$W(\vec{q},\vec{p}) = \frac{1}{\pi\hbar}\int d\eta \Psi^*(\vec{q}+\frac{\vec{\eta}}{2})\Psi(\vec{q}-\frac{\vec{\eta}}{2})e^{\frac{\vec{\eta}\cdot\vec{p}}{\hbar}}, \tag{26}$$

where $\vec{q}$ and $\vec{p}$ are coordinates and conjugated momenta. The Wigner function has many appealing features which suggest it as a good candidate for a classical phase-space representation of the wavefunction. Namely

$$\int d\vec{p}W(\vec{q},\vec{p}) = |\Psi(\vec{q})|^2, \tag{27}$$

$$\int d\vec{q}W(\vec{q},\vec{p}) = |\Psi(\vec{p})|^2, \tag{28}$$

$$\left\langle \hat{A}(\vec{q},\vec{p}) \right\rangle = \int d\vec{q} \int d\vec{p} A(\vec{q},\vec{p},t)F(\vec{q},\vec{p},t), \tag{29}$$

but, most importantly, the time evolution equations for the Wigner function collapse to classical Hamilton equations in the limit $\hbar \to 0$ [20]. The price is that the Wigner distribution function is not necessarily always positive.

We have taken the initial coordinates and momenta for the swarm of trajectories from the Wigner distribution. It can be easily proven that for a separable wavefunction the Wigner function can be written in a product form. As a basis for photodissociation calculations we have used a wavefunction in the form 4, therefore, the corresponding Wigner distribution is given by an expression

$$\begin{aligned} &P(q_1,...,q_{3N-6},\rho,\phi,\theta,p_1,...,p_{3N-6},p_\rho,J_z,p_z\rho) \propto \\ &e^{-\omega_1({q_1}^2+{p_1}^2)}...e^{-\omega_{3N-6}({q_{3N-6}}^2+{p_{3N-6}}^2)}\frac{P^{HX,vib}(\rho,p_\rho)}{\rho^2}P^{HX,rot}(\phi,\theta,J_z,p_z\rho). \end{aligned} \tag{30}$$

Here, $p_i$ is the momentum coordinate of a cage mode $i$, $p_\rho$ is the momentum in the HX vibrational coordinate, $J_z$ and $p_z\rho$ are conjugated momenta to the polar angles $\phi$ and $\theta$, respectively. $J_z$ is the projection of the total angular momentum onto the z-axis and $p_z\rho$ is the momentum in the z-axis multiplied by the radius. $P^{HX,vib}$ and $P^{HX,rot}$ are the Wigner quasi-probabilities for the degrees of freedom of the HCl molecule.

Once the initial coordinates, momenta, and weights are generated, a swarm of classical trajectories is propagated by numerically solving the Newton equations of motion [32] in a standard way [2]. Typically, several hundreds trajectories are required for converged results.

If we impose an assumption that the chromophore molecule is excited by an ultrashort laser, then the pulse covers all the frequencies. Consequently, the whole initial wavefunction is promoted to the excited state. In the experiment, however, a cw laser with a fixed wavelength is usually used. Within the Wigner trajectories approach we have, therefore, to filter the Wigner distribution function in such a way that the energetic relation

$$\hbar\omega = E^{e}_{Rg-HX} - E^{g}_{Rg-HX} \tag{31}$$

is fulfilled. Here, $\hbar\omega$ is the energy of the exciting photon, $\mathrm{E}^{g}_{Rg-HX}$ and $\mathrm{E}^{e}_{Rg-HX}$ are the interaction energies between argons and HX in the ground and in the excited states. Note that quantum dynamics simulation of photodissociation process with a cw laser field would require incorporating the laser field into a molecular Hamiltonian. The difference between a simulation with an ultrashort excitation time and that with a fixed wavelength can be rather pronounced, namely when the wavelength excites the blue or the red tail of the ground state wavefunction.

### 3.4. NON-ADIABATIC DYNAMICS

After the HX molecule is promoted into a specific electronic state, it evolves and can also relax back to the ground electronic state via a non-adiabatic transition. It ha been referred [**?**] that non-adiabatic transitions can play an important role for large HCl-$\mathrm{Ar}_n$ systems. Within the DIM approach it is possible to construct not only the potential energy surfaces of the excited states but also non-adiabatic couplings. Then the dynamics can proceed via a semiclassical surface hopping algorithm as proposed by Tully [47].

## 4. Analysis

### 4.1. QUANTITIES IN TIME AND ENERGY DOMAINS

The result of a molecular dynamics simulation is a time dependent wavefunction (quantum dynamics) or a swarm of trajectories in a phase space (classical dynamics). To analyze what are the processes taking the place during photodissociation one can directly look at these. This analysis is, however, impractical for systems with a high dimensionality. We can calculate either quantities in the time domain or in the energy domain. In the time domain survival probabilities can be measured by pump-probe experiments [52], in the energy domain the distribution of the hydrogen kinetic energy can be experimentally obtained [9].

In the case of our systems it is in principal possible to measure the probability of hydrogen to stay in the cluster. In the molecular dynamics simulation the survival probability is calculated by integrating the square of the wavefunction over the cluster region

$$P(t) = \int_{\text{cluster}} |\Psi_f(\vec{r},t)|^2 \,\mathrm{d}\vec{r}, \tag{32}$$

where $\Psi_f(\vec{r},t)$ is the time-dependent hydrogen wavepacket. In classical simulations we simply count at each the number of trajectories localized in the cluster region. The cluster region we define as a sphere to a radius corresponding with the cluster size.

In the energy domain, one can calculate the final distribution $P(E)$ of the kinetic energy of the hydrogen outgoing from the cluster (KED spectrum). While the calculation of this quantity within the classical framework is straightforward (simply we do a histogram of the final kinetic energies), the calculation of this quantity from wavepackets deserves a small remark. The KED spectrum is given as

$$\begin{aligned} \lim_{t\to\infty} P(E_{\text{kin}},t) &= \lim_{t\to\infty} \frac{1}{\left|\vec{k}\right|} \int \left| \left\langle \exp\left(i\vec{k}\vec{r}\right) | \Psi_f\left(\vec{r},t\right) \right\rangle \right|^2 \sin(\theta_k)\mathrm{d}\theta_k \mathrm{d}\phi_k, \\ |\vec{k}|^2 &= 2mE_{\text{kin}}\frac{1}{\hbar^2}, \end{aligned} \tag{33}$$

where $\Psi_f$ is hydrogen wavefunction moving on the excited surface, $\vec{k}$ is the momentum of hydrogen divided by the Planck constant, $\vec{r}$ is the coordinate of hydrogen, and $m$ is the hydrogen mass. It can be shown that

$$\lim_{t\to\infty} P(E_{\text{kin}},t) = \int_{-\infty}^{\infty}, \langle \Psi(\vec{r},t=0)|\Psi(\vec{r},t)\rangle \exp\left(\frac{i}{\hbar}E_{\text{kin}}t\right) \mathrm{d}t, \tag{34}$$

which is actually nothing else than a Fourier transform of an autocorrelation function. This prescription is (except of the prefactor) identical with that for absorption or emission spectrum [18]. The recurrences in the time domain correspond to resonances in the energy domain. These phenomena are not apparent in the classical framework.

### 4.2. SCATTERING OF HYDROGEN ATOMS FROM THE CAGE AND MIXING OF ELECTRONIC STATES

The direct comparison of calculations and experiment is more complicated for systems which are excited into more than one electronically excited state depending on laser polarization, e.g. in the case of HI where the system is excited to three states corresponding either with ground or excited spin orbit state I and I*. We define a branching fraction

$$\Gamma = \frac{[I*]}{[I]+[I*]}. \tag{35}$$

The measured kinetic energy distribution spectrum $P(E)$ is then actually a functional of the two dimensional kinetic energy distributions $P_g(E,\Theta_S)$ and $P_e(E,\Theta_S)$ (where index g denotes ground spin orbit state, e excited spin orbit state and $\Theta_S$ is a scattering angle of the photodissociated hydrogen). Without going into details [41], the measured KED spectrum is given as:

$$\begin{aligned} P(E) = \frac{1}{2}(1-\Gamma)\int_0^{2\pi}\int_0^{\pi} \sin\Theta_E P_g(\Theta_D,E)\sin^2(\Theta_E)d\Theta_E d\phi_E \\ +\Gamma\int_0^{2\pi}\int_0^{\pi} \sin\Theta_E P_e(\Theta_D,E)\cos^2(\Theta_E)d\Theta_E d\phi_E \end{aligned} \tag{36}$$

where the angle $\Theta_D$ is related to the $\Theta_E$ depending on the laser polarization used.

Thus, we can obtain not only energetic information but by comparing the calculation with the experiment also an information on scattering characteristics of the photodissociated hydrogen atoms. Let us show this on an example of HI-$Ar_147$ cluster. Here we assume two dopant positions, either in the second (sub-surface) shell, or in the surface shell. The overall KED integrated over all scattering angles are almost identical for these two cases. However, two-dimensional plots of $P_g(E,\Theta_S)$ and $P_e(E,\Theta_S)$ are completely different for these two isomers (see Fig. 8).

After processing the two dimensional KEDs according to eq. 36, we can directly compare the calculations with the experiment. In Fig. 9 we can see that while we have a very good agreement for a surface isomer for both polarizations measured, this agreement is lost for the sub-surface isomer. This strongly suggests that the true position of the HI is in the surface substitutional position.

## 5. Simulation of experiment and control

### 5.1. SIZE AND SITE CONTROL

Size of the cluster as well as the position of the dopant can significantly change the character of the photodissociation. We show this effect on the example of the HBr-$Ar_n$ clusters. Fig. 10 depicts these survival probabilities for embedded (surface) isomers of different sizes initially in the ground rotational (librational) state of HBr. There is a dramatic difference in the decay of the hydrogen population in the cage between the two smaller and

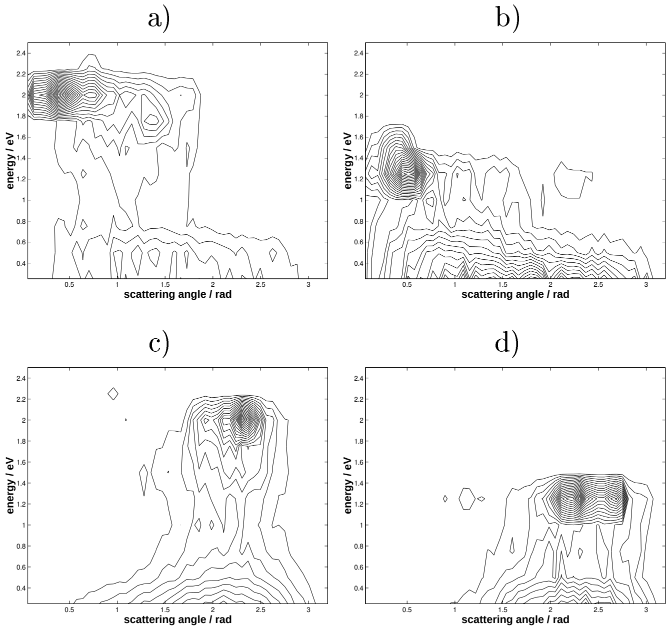


*Figure 8.* Angular and kinetic energy distribution of the outgoing hydrogen atoms. Graphs a) and c) corresponds to the H + I exit channel, while b) and d) with the H + I* channel. In the case a) and b) the dopant is placed in the second shell, while in the case c) and d) the dopant is on the surface.

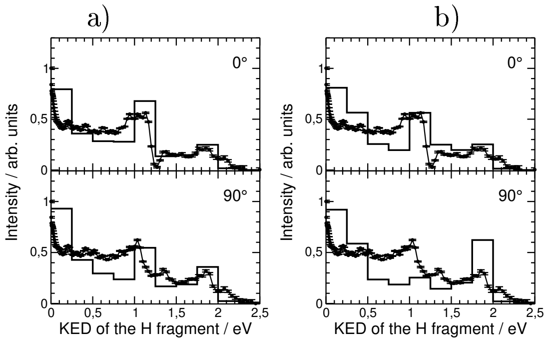


*Figure 9.* a) Simulation of the photodissociation of the dopant on the surface (histogram) compared with a pick-up photodissociation experiment (line with error bars). b) Simulation of the photodissociation of the dopant in the sub-surface shell (histogram) compared with a pick-up photodissociation experiment (line with error bars).

the larger clusters with embedded HBr. Figure 10a clearly shows that the first two solvation layers are quite inefficient in caging, which only becomes

a) b)

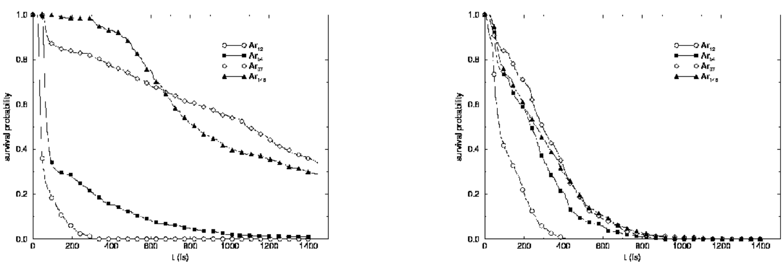

*Figure 10.* a)Transient probabilities of finding the photodissociating hydrogen inside the cluster for embedded $HBr(Ar)_n$ ($n$=12-146) isomers. b) Transient probabilities of finding the photodissociating hydrogen inside the cluster for embedded $HBr(Ar)_n$ ($n$=12-146) isomers.

strong after the third argon layer starts to build up. The size dependence is much weaker for surface isomers where we see a continuous increase of the transient survival probabilities upon enlarging the cluster.

KED spectra for $HBr(Ar)_{12}$, $HBr(Ar)_{54}$, $HBr(Ar)_{97}$, and $HBrAr_{146}$ are depicted in Figs. 11 -14. For each cluster size two KED spectra have been evaluated, corresponding to the embedded or surface isomer. The KED spectra for these two isomers differ significantly from each other at each size. Note, that caging is very inefficient for the embedded isomer of $HBr(Ar)_{12}$. As a result, high energy peaks at 1.3 and 0.9 eV, corresponding to directly exiting hydrogens for the Br and Br* channels, represent the main features in the KED. Upon adding more argon atoms, a peak at zero hydrogen velocity, which corresponds to efficient caging, starts to grow and finally dominates the spectrum. For large embedded isomers, we see only a small component of fast hydrogen for the $HBr(Ar)_{97}$ cluster with a half-filled third solvation layer and zero intensity at high kinetic energies for the $HBr(Ar)_{146}$ cluster with three complete solvation layers. In contrast, the KEDs for surface isomers change only slightly upon increasing the cluster size from 12 to 146 argon atoms. Even for the smallest surface isomer under study, the $HBr(Ar)_{12}$ cluster, caging is efficient and, consequently, a significant signal at zero kinetic energy is observed. The results for the three larger surface isomers are very similar. The dominant signal appears at zero velocity, however, the fast hydrogen component does not vanish even for the largest cluster. Effectively, HBr deposited on the argon cluster surface is surrounded by more argon "solvation layers", than for the embedded isomer of the same size. On the other hand, some trajectories corresponding to tails

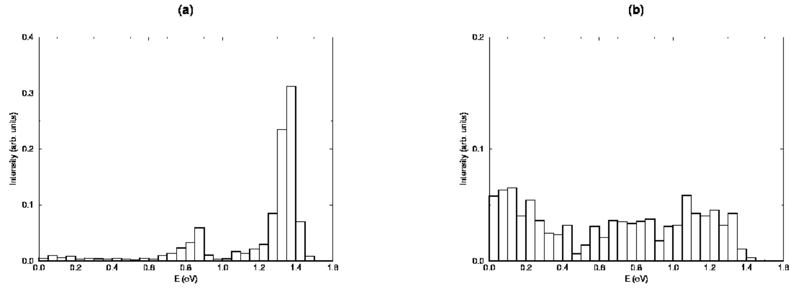

*Figure 11.* Final kinetic energy distributions of the photolyzed hydrogen for the a) embedded and b) surface isomers of $HBr(Ar)_{12}$.

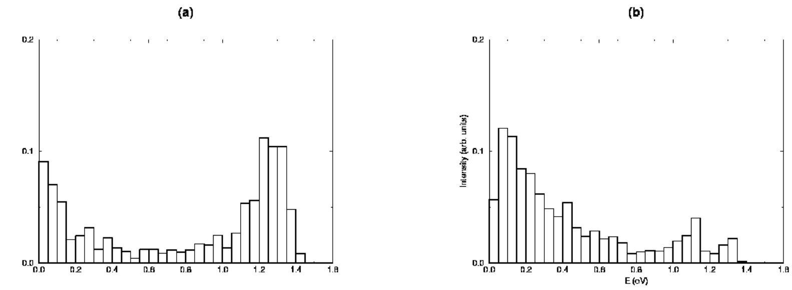

*Figure 12.* Final kinetic energy distributions of the photolyzed hydrogen for the a) embedded and b) surface isomers of $HBr(Ar)_{54}$.

of the librational wavefunctions do not penetrate into the argon cluster.

The experimental results depicted on Fig. 15 can be readily compared with simulations of $HBr(Ar)_{54}$ to $HBr(Ar)_{146}$ clusters depicted at Figs. 12 to 14. It is obvious that all the trends both for the embedded an for the surface isomers are well reproduced by the MD simulation. Namely that for a surface isomers, only a weak size dependence of the KED spectra is observed, while strong dependence on the cluster size is recorded for the embedded isomer. Note, that the experiment generates clusters with a certain size distribution and also that for smaller clusters there are rather pronounced error bars in the experiment. This can explain small differences between experiment and simulation in the sharpness of the peaks in the KED spectra, especially for the embedded case. Note also that in the case of surface isomer also different clusters with different dopant positions can

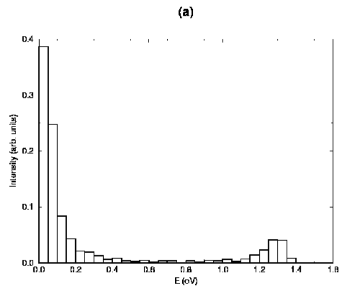

*Figure 13.* Final kinetic energy distributions of the photolyzed hydrogen for the a) embedded and b) surface isomers of $HBr(Ar)_{97}$.

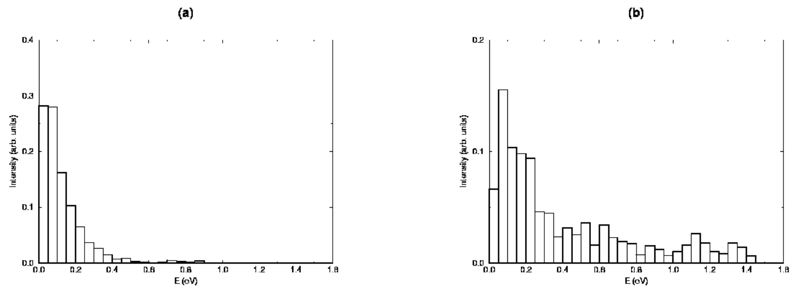

*Figure 14.* Final kinetic energy distributions of the photolyzed hydrogen for the a) embedded and b) surface isomers of $HBr(Ar)_{146}$.

contribute and can enhance the fast component of the KED spectrum [7].

### 5.2. LIBRATIONAL CONTROL

The control scheme of librational control [24] relies on the following scheme

$$\begin{aligned} AB + h\nu(IR) &\longrightarrow AB(v>0) \\ AB(v>0) + h\nu(UV) &\longrightarrow AB* \\ AB* &\longrightarrow A(\alpha) + B(\beta), \end{aligned} \tag{37}$$

where $AB(v > 0)$ denotes the vibrationally excited AB molecule in its ground state and AB* is the electronically excited AB molecule. The initial wavefunction can have different spatial orientations and by choosing the

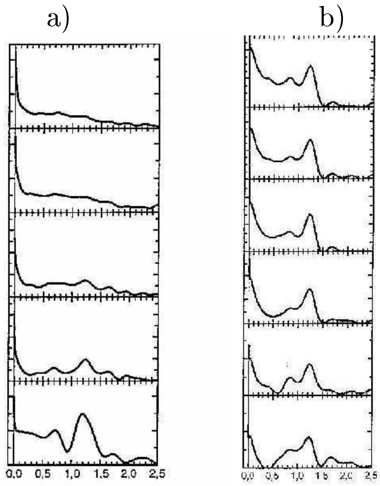


*Figure 15.* Experimental kinetic energy distributions of the photolyzed hydrogen for the a) embedded and b) surface isomers of $HBr(Ar)_n$ with a mean value of $\overline{n}$ changing gradually from 55 (lower graphs) to 139 (upper graphs).

proper vibrationally excited state we can determine the photodissociation results. This principle is demonstrated on the HCl-$Ar_n$ system [55].

In all clusters there exist low-lying excited librational states, where most of the hydrogen wavefunction is oriented away from the cluster or at least sidewise. This is demonstrated in Fig. 16 for the case of the $HCl(Ar)_{12}$ complex. For these excited librational states caging becomes inefficient since the photodissociating hydrogen minimizes the interaction with the argon cage. In other words, librational preexcitation can be used to "turn off" the cage effect for surface solvated hydrogen halides.

Among of the systems under study, clusters with three, five, six and twelve atoms possess higher symmetries having more than a twofold rotational axis. As a result doubly degenerate librational states occur in these complexes. In Fig. 16 one of the possible representations of these degenerate states in the $HCl(Ar)_{12}$ cluster is displayed, however, any linear combination of these functions is also valid.

Three pronounced recurrences shown in Fig. 17a demonstrate repeated collisions of hydrogen with the cluster. The situation becomes dramatically different for photolysis started from the first non-degenerate librationally excited state. In this state most of the initial hydrogen density is oriented sidewise with respect to the cage (see Fig. 16b). As a results caging becomes very inefficient and, consequently only a single recurrence occurs during the dynamics (see Fig. 17b).

From the point of view of measurable quantities, this is manifested in

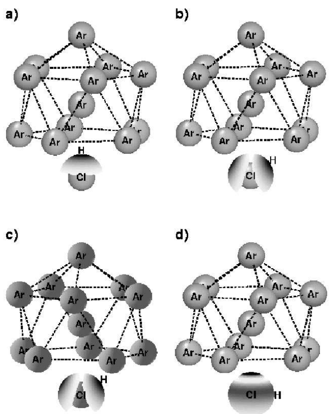


*Figure 16.* a) Ground and b)-c) lowest excited librational wavefunctions of the HCl molecule deposited on clusters with twelve argon atoms. The shadowing represents the angular hydrogen probability and the wired spheres correspond to effective radii of the heavy atoms. Note the structures b) and c) corresponding to a degenerate pair of functions. For the sake of clarity, the radius of the hydrogen sphere is artificially expanded.

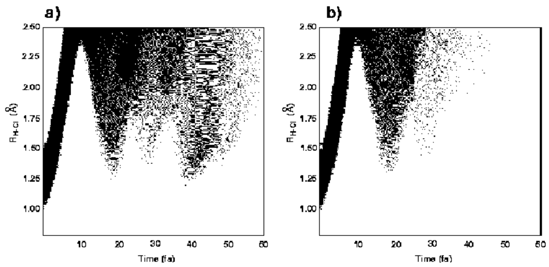


*Figure 17.* Quantum dynamics of the radial hydrogen wavepacket motion for HCl photolysis on the $Ar_{12}$ cluster initiated from the a) ground, b) first non-degenerate excited librational state.

a following way. Fig. 18 shows the KED spectra for HCl photolysis on the $Ar_{12}$ cluster, initiated either from the ground or from the first non-degenerate excited librational state. In the former case strong caging results in a well developed vibrational structure in the KED. This means that a significant part of the hydrogen wavefunction lives for nearly 100 fs in the cage and repeatedly returns to the Franck-Condon region. Clearly, the resonant structure is the strongest among the systems under study. It is even stronger than in the case of a rotationally cold photodissociating HCl molecule fully solvated in the $Ar_{12}$ cluster. On the other hand, the structure in the KED disappears upon librational preexcitation, which orients most of the photodissociating hydrogen away from the argon cluster.

For the possible experimental realization of librational control it is important to take into account energy considerations. Our calculations show that the level spacing between the ground and lowest excited librational state amounts to 35-70 $cm^{-1}$. Thus, for efficient discrimination between the librational states the cluster temperature should not exceed few tens of Kelvins. This is realistic for the cluster sizes investigated here. For larger clusters, where higher temperatures might cause a problem, the technique of embedding in helium droplets, which leads to a very efficient cooling, could in principle be employed. Another point is which experimental observable should be used as a fingerprint of the librational control mechanism. Here, we suggest to monitor the disappearance of the resonant structure in the hydrogen KED upon librational preexcitation. The present setup corresponds to an ultrashort (therefore, energetically broad) exciting UV pulse. Another option is to use a longer (nanosecond) pulse with a frequency at the low energy tail of the hydrogen halide absorption band. Such an excitation produces a much less energetic hydrogen, which is more efficiently trapped in the argon cage. An observable consequence of librational preexcitation is then a disappearing low energy part of the KED, corresponding to caged hydrogens.

### 5.3. EXTERNAL ELECTRIC FIELD

The librational wavefunction delocalization can be efficiently controlled by a direct current electric field [21]. The dipole moment of the HX molecule is coupled to the external electric field by a factor $-\vec{\mu}.\vec{E}$ in the the Hamiltonian. The higher the intensity of the electric field, the more classically the system behaves. The principle is demonstrated for the case of the Ne-HI molecule 19. This molecule has a vibrationally averaged structure corresponding to a secondary minimum (DMC wavefunction in Fig. 19a). If we apply an electric field of the intensity $2.5 \times 10^5$ V/cm, the librational wavefunction becomes more classical but still the structure is not covering the

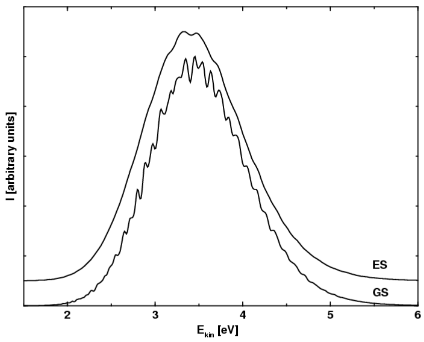


*Figure 18.* Kinetic energy distributions of hydrogen atoms produced from photolysis of HCl@$Ar_{12}$ started from the ground (GS) or first non-degenerate excited (ES) librational states of the HCl molecule. For clarity, the spectra are arbitrarily vertically shifted with respect to each other.

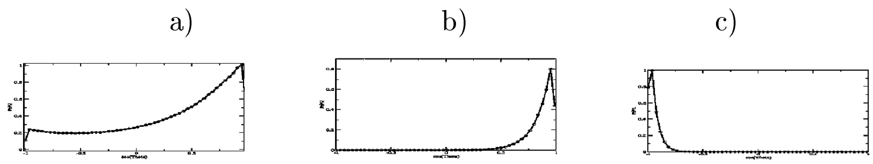


*Figure 19.* Structure control of a Ne-HBr cluster by a DC electric filed. x-axis: $\cos\Theta$, y-axis: wavefunction($\Theta$ is the angular part of the Jacobi coordinate system).

global minimum on the potential energy surface. An electric field of the intensity of $2.5.10^6$ V/cm flips the wavefunction, so that the other isomer is formed. Note that unlike for the ground state no cage effect would be observed for this second minimum. For smaller fields applied, the cage effect would be, however, more pronounced. One could observe in this case long living resonances.

## 6. Conclusions

In this chapter we have described the way how to simulate the photodissociation dynamics in large, cryogenic clusters. We have emphasized the role of the initial conditions for the correct description of the experimental quantities. Preparing the system in different initial states is also a way how to control the photodissociation process. We can tune the cage effect by changing cluster size, the site of the chromophore, by librational preexcitation, by an external electric field, by cluster composition of by changing the temperature of the clusters. All these control exploits the the orientation by weak intermolecular forces. We have shown that for the dynamical description usually the classical mechanics within the Wigner trajectories approach is sufficient.

ACKNOWLEDGMENT

Support of the Czech Ministry of Education to the Center for Complex Molecular Systems and Biomolecules (Grant No. LN00A032) is gratefully acknowledged.

## References

1. Alimi, R. and R. Gerber: 1990, 'Solvation Effects on Chemical Reaction Dynamics in Clusters: Photodissociation of HI in $Xe_nHI$'. *Phys. Rev. Lett.* **64**, 1453–1456.
2. Allen, M. P. and D. J. Tildesley: 1987, *Computer Simulations of Liquids.* Clarendon Press, Oxford.
3. Anderson, D., S. Davis, and D. Nesbitt: 1997, 'Sequential solvation of HCl in argon: High resolution infrared spectroscopy of $Ar_nHCl(n=1,2,3)$'. *J. Chem. Phys.* **107**, 1115–1127.
4. Aques, C., L. Valachovic, S. Iionov, E. Bohmer, Y. Wen, J. Segall, and C. Wittig: 1993, 'Photoinitiated processes in complexes - subpicosecond studies of co2-hi and stereospecificity in Ar-HX'. *J. Chem. Soc. Faraday T* **89**, 1419–1425.
5. Auer, B. M. and A. B. McCoy: 2003, 'Using diffusion Monte Carlo to evaluate the initial conditions for classical studies of the photodissociation dynamics of HCl dimer'. *J. Phys. Chem. A* **107**, 4–12.
6. Barnett, R. N., P. J. Reynolds, and W. A. Lester: 1991, 'Monte-carlo algorithms for expectation values of coordinate operators'. *J. Comput Phys.* **96**, 258–276.
7. Baumfalk, R., N. Nahler, U.Buck, M. Niv, and R. Gerber: 2000, 'Photodissociation of HBr adsorbed on the surface and embedded in large $Ar_n$ clusters'. *J. Chem. Phys.* **113**(1), 329–338.
8. Berne, B. J. and D. Thirumalai: 1986, 'On the simulation of quantum systems: Path integral methods'. *Annu. Rev. Phys. Chem.* **37**, 401.
9. Buck, U.: 2002, 'Photodissociation of hydrogen halide molecules in different cluster environments'. *J. Phys. Chem.* **106**, 10050–10062.
10. Castillo-Chara, J., R. R. Lucchese, and J. W. Bevan: 2001, 'Differentiation of the ground vibrational and global minimum structures in the Ar : HBr intermolecular complex'. *J. Chem. Phys.* **115**, 899–911.
11. Chakravarty, C.: 1995, 'Melting of neon clusters - path integral Monte Carlo simulations'. *J. Chem. Phys.* **102**, 956–962.
12. Dickey, J. M. and A. Paskin: 1969, 'Computer simulation of the lattice dynamics of solids'. *Phys. Rev.* **188**, 1407–1418.
13. Donoso, A. and C. C. Martens: 2001, 'Quantum tunneling using entangled classical trajectories - art. no. 223202'. *Phys. Rev. Lett.* **8722**, (22) 3202–+ NOV 26 2001.
14. Ellison, F. O.: 1996, 'A method of Diatomics in Molecules. I. General theory and applications'. *J. Am. Chem. Soc.* **85**, 3540–3544.
15. Feynman, R. P. and A. R. Hibbs: 1965, *Quantum Mechanics and Path Integrals.* New York: McGraw Hill.
16. García-Vela, A.: 1998, 'Study of the total and partial fragmentation dynamics of

Ar-HCl after UV photodissociation'. *J. Chem. Phys.* **108**, 5755.
17. Gerber, R. B., R. Kosloff, and M. Ratner: 1986, 'Time dependent wavepacket calculations of molecular scattering from surfaces'. *Comp. Phys. Rep.* **5**, 59–113.
18. Heller, E.: 1981, 'The semiclassical way to molecular spectroscopy'. *Acc. Chem. Res.* **14**, 368–375.
19. Herzberg, G.: 1950, *Molecular Spectra and Molecular Structure.* New York: Van Nostrand.
20. Hillery, M., R. F. O'Connel, M. O. Scully, and E. P. Wigner: 1984, 'Distribution functions in physics - fundamentals'. *Phys. Rep.* **106**, 121–167.
21. Hinde, R. J.: 1998, 'Structural control of Ar-HF complexes using dc electric fields: a diffusion quantum Monte Carlo study'. *Chem. Phys. Lett.* **283**, 125–130.
22. Jungwirth, P. and R. B. Gerber: 1995, 'Quantum dynamics of large polyatomic systems using a classically based separable potential method'. *J. Chem. Phys.* **102**, 6046–6056.
23. Jungwirth, P. and R. B. Gerber: 1999, 'Quantum molecular dynamics of ultrafast processes in large polyatomic system's'. *Chem. Rev.* **99**, 1583–1606.
24. Jungwirth, P., P. Žďánská, and B. Schmidt: 1998, 'Librational control of photochemical reactions in small clusters'. *J. Phys. Chem. A* **102**, 7241–7244.
25. Kalos, M. H.: 1967, 'Stochastic Wave Function for Atomic Helium'. *J. Comp. Phys.* **2**, 257.
26. Kosloff, R.: 1994, 'Propagation methods for quantum molecular dynamics'. *Annu Rev. Phys. Chem.* **45**, 145–178.
27. Leake, J. A., W. B. Daniels, J. J. Skalyo, B. C. Frazer, and G. Shirane: 1969, 'Lattice dynamics of neon at two densities from coherent inelastic neutron scattering'. *Phys. Rev.* **181**, 1251–1260.
28. Lepetit, B. and D. Lemoine: 2002, 'State-to-state ArHBr photodissociation quantum dynamics'. *J. Chem. Phys.* **117**, 8676–8685.
29. McIntosh, A., Z. Wang, J. Castillo-Chara, R. R. Lucchese, J. Bevan, R. D. Suenram, and A. C. Legon: 1999, 'The structure and ground state dynamics of Ar-IH'. *J. Chem. Phys.* **111**, 5764–5770.
30. Monnerville, M. and B. Pouilly: 1998, 'First Quantum Investigation of the Photodissociation of the Ar-HBr Complex: Three-dimensional Time-dependent Approach'. *Chem. Phys. Lett.* **294**, 473–479.
31. Narevicius, E. and N. Moiseyev: 1998, 'Structured photo-absorption spectra of ArHCl: fingerprints of overlapping broad resonances'. *Chem. Phys. Lett.* **287**, 250–254.
32. Newton, I.: 1687, *Philosophia Naturalis Principia Mathematica.* London.
33. Niv, M., A. Krylov, and R. Gerber: 1997, 'Photodissociation, Electronic Relaxation and Recombination of HCl in $Ar_n$(HCl) Clusters: Nonadiabatic Molecular Dynamics Simulations'. *Faraday Discussions* **108**, 243–254.
34. Niv, M. Y., A. I. Krylov, R. B. Gerber, and U. Buck: 1999, 'Photodissociation of HCl adsorbed on the surface of an $Ar_1 2$ cluster: Nonadiabatic molecular dynamics simulations'. *J. Chem. Phys.* **110**, 11047.
35. Perera, L. and F. G. Amar: 1990, 'Spectral shifts and structural classes in microsolutions of rare gas clusters containing a molecular chromophore'. *J. Chem. Phys.* **93**, 4884–4897.
36. Portwich, G.: 1995. Master's thesis, Universität Göttingen.
37. Schmidt, B.: 1999, 'Quantum dynamics of HF photodissociation in icosahedral $Ar_{12}HF$ clusters: rotational control of the hydrogen cage exit'. *Chem. Phys. Lett.* **301**, 207.
38. Schröder, T., R. Schinke, S. Liu, Z. Bacic, and J. Moskowitz: 1995, 'Photodissoziation of HF in $Ar_nHF$ (n=1-14,54) Van der Waals Clusters: Effects of the Solvent Cluster Size on the Solute Fragmentation Dynamics'. *J. Chem. Phys.* **103**, 9228–9241.
39. Segall, J., Y. Wen, R. Singer, C. Wittig, A. García-Vela, and R. Gerber: 1993, 'Evidence for a Cage Effect of HBr in Ar-HBr. Theoretical and Experimental Results'.

*Chem. Phys. Lett.* **207**, 504–509.

40. Sese, L. M.: 1994, 'Study of the feynman-hibbs effective potential against the path-integral formalism for monte-carlo simulations of quantum many-body lennard-jones systems'. *Mol. Phys.* **81**, 1297–1312.
41. Slavíček, P., P. Jungwirth, M. Lewerenz, N. H. Nahler, M. Farnik, and U. Buck: 2003, 'Photodissociation of HI on the surface of large argon clusters: The orientation of the librational wavefunction and the scattering from the cluster cage'. *J. Chem. Phys.* p. submitted.
42. Slavíček, P., M. Roeselová, P. Jungwirth, and B. Schmidt: 2001, 'Preference of cluster isomers as a result of quantum delocalization: Potential energy surfaces and intermolecular vibrational states of Ne$\cdots$HBr, Ne$\cdots$HI, and $HI(Ar)_n$ (n = 1 – 6)'. *J. Chem. Phys.* **114**(4), 1539–1548.
43. Slavíček, P., P. Žďánská, P. Jungwirth, R. Baumfalk, and U. Buck: 2000, 'Size Effects on Photodissociation and Caging of Hydrogen Bromide Inside or on the Surface of Large Inert Clusters: From One to Three Icosahedral Layers'. *J. Phys. Chem. A* **104**, 7793–7802.
44. Sterling, M., Z. Li, and V. A. Apkarian: 1995, 'Simulations of quantum crystals by classical dynamics'. *J. Chem. Phys.* **103**, 5679–5683.
45. Stratt, R. M.: 1995, 'The instantaneous normal-modes of liquids'. *Accounts Chem. Res* **28**, 201–207.
46. Trin, J., M. Monnerville, B. Pouilly, and H. D. Meyer: 2003, 'Photodissociation of the ArHBr complex investigated with the multiconfiguration time-dependent Hartree approach'. *J. Chem. Phys.* **118**, 600–609.
47. Tully, J. C.: 1990, 'Molecular-dynamics with electronic-transitions'. *J. Chem. Phys.* **93**, 1061–1071.
48. Vach, H.: 1999, 'Impurity dynamics in binary van der Waals clusters created by pick-up'. *J. Chem. Phys.* **111**, 3536–3547.
49. Vach, H.: 2000, 'Solvation effects in large binary van der Waals clusters with high doping rates'. *J. Chem. Phys.* **113**(3), 1097–1103.
50. von Pietrowski, R., M. Rutzen, K. von Haeften, S. Kakar, and T. Möller: 1997, 'Fluorescence excitation spectroscopy of xenon doped neon clusters: size and site effects, and cluster melting'. *Z. Phys. D* **40**, 22–24.
51. Wales, D., J. Doye, M. Miller, P. Mortenson, and T. Walsh: 2000, 'Energy landscapes: from clusters to biomolecules'. *Adv. Chem. Phys.* **115**, 1–111.
52. Willberg, D. M., M. Gutmann, J. J. Breen, and A. H. Zewail: 1992, 'Real time dynamics of clusters 1.: $I_2X_n$ (n=1)'. *J. Chem. Phys.* **96**, 198–212.
53. Žďánská, P. and N. Moiseyev: 2001, 'Phases and amplitudes of recurrences in autocorrelation function by a simple classical trajectory method'. *J. Chem. Phys.* **115**, 10608–10620.
54. Žďánská, P., B. Schmidt, and P. Jungwirth: 1999, 'Photolysis of hydrogen chloride embedded in the first argon solvation shell: Rotational control and quantum dynamics of photofragments'. *J. Chem. Phys.* **110**, 6246–6256.
55. Žďánská, P., P. Slavíček, and P. Jungwirth: 2000, 'HCl photodissociation on argon clusters: Effects of sequential solvation and librational preexcitation'. *J. Chem. Phys.* **112**(24), 10761–10766.